Supplementary Information

Cobalt-platinum intermetallic composite loaded on pyridinic N-enriched carbon for acidic hydrogen evolution catalysis with ultralow overpotential

Qiushi Xie[#], Jiankun Li[#], Keyu Wang, Shiyi Li, Weiyi Xu, Yixing Wang, Linfeng Lei, Siyao Li, Linzhou Zhuang*, Zhi Xu*

State Key Laboratory of Chemical Engineering, School of Chemical Engineering, East China University of Science and Technology, Shanghai, 200237, China

Email: zhixu@ecust.edu.cn, lzzhuang@ecust.edu.cn

Characterization

X-ray Powder Diffraction (XRD) data was collected on a Bruker D8 Advance X-ray Polycrystalline Diffractometer at 40 kV/40 mA with Cu Ka radiation (k = 1.541874 Å) in the angular range of 5–80° for the 2h angle. The transmission electron microscope images were taken on a HRTEM JEOL 2100F. X-ray photoelectron spectroscopy (XPS) analysis was carried out on a Thermo ESCALAB 250Xi using an aluminum monochromatic X-ray source (hv = 1486.6 eV, power = 150 W).

DFT calculation methods

DFT calculation were performed using the Vienna ab initio simulation package (VASP). The exchange-correlation interaction was described by the generalized gradient approximation (GGA) with the revised Perdew–Burke–Ernzerhof (PBE)

functional. The kinetic cutoff energy of 450 eV and Gamma-centered k-points of 3 × 3 × 1 were used. Besides, all atoms were fully relaxed until the energies and residual forces on each atom converged to 1×10^{-5} eV and 0.02 eV·Å^{-1}. For construction of the surface models, a vacuum of 15 Å was used to eliminate interactions between periodic structures.

ΔG_H^* was defined as $\Delta G_H^* = \Delta E_H^* + \Delta E_{ZPE} - T\Delta S_H$. ΔE_H^* is the hydrogen chemisorption energy expressed by the following equation: $\Delta E_H^* = E_{(Slab-H^*)} - E_{(Slab)} - \frac{1}{2}E_{H2}$[1]. $E_{(Slab-H^*)}$ and $E_{(Slab)}$ are the energies of the active sites with and without H* absorption, respectively. ΔE_{ZPE} is the zero-point energy difference between the adsorbed and gas phases. ΔS_H is the entropy change between the adsorbed H and gas-phase H_2 at 1 atm and T is 298.15 K. The sum of them, which could be regarded as thermal correction to Gibbs free energy, could be obtained via vibrational frequency calculations. In this work, we defined the ΔG_H^* values as ΔE_H^* + 0.24eV for all catalysts. VASPKIT[2] was used to directly read the value from OUTCAR file.

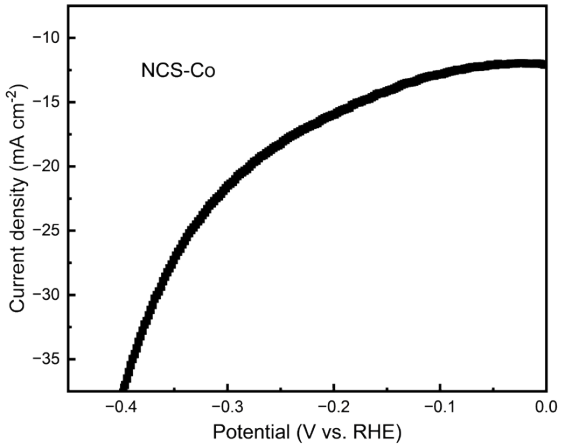

Fig. S1 HER performance of NCS-Co

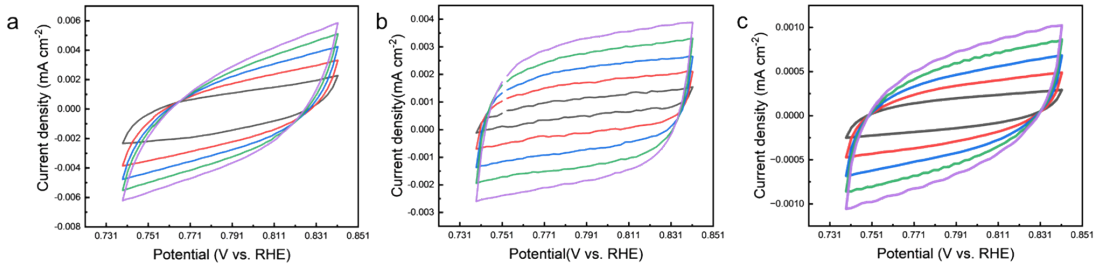

Fig. S2 Cyclic voltammograms in 0.5 M H_2SO_4 at the scan of 20-100 mV/s in non-faradaic region for (a) NCS-CoPt, (b) NCS-CoPt-H, (c) NCS-Co, respectively.

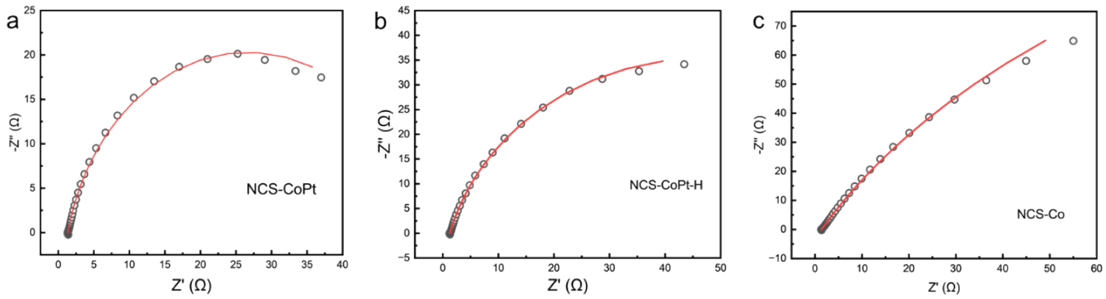

Fig. S3 Nyquist plot of (a) NCS-CoPt, (b) NCS-CoPt-H, (c) NCS-Co

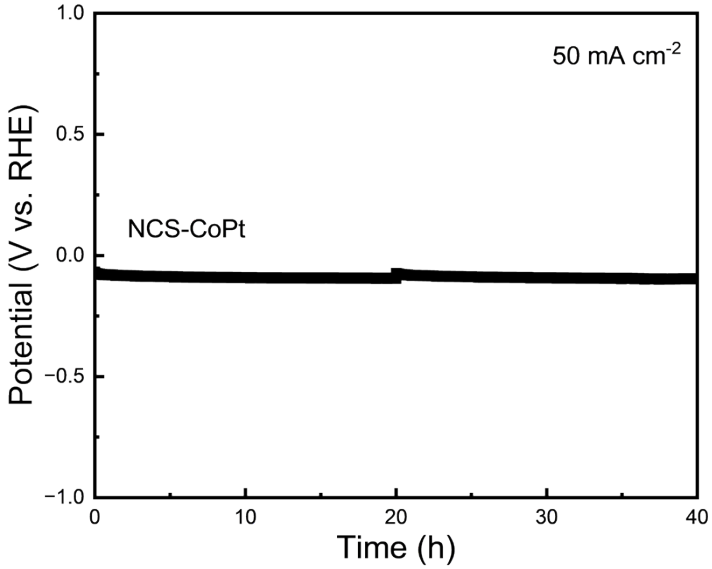

Fig. S4 Stability test of NCS-CoPt at the current density of 50 mA cm^{-2} in 0.5 M H_2SO_4.

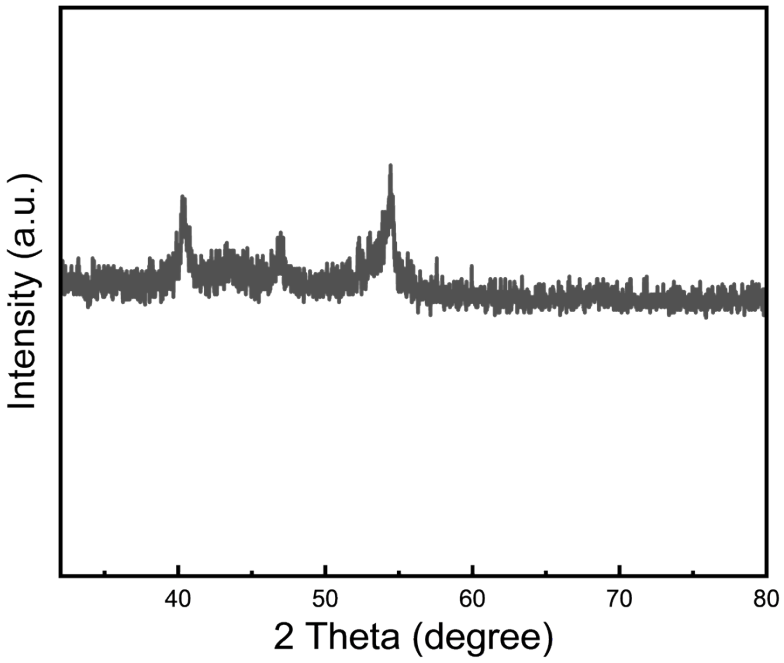

Fig. S5 XRD of NCS-CoPt after stability test

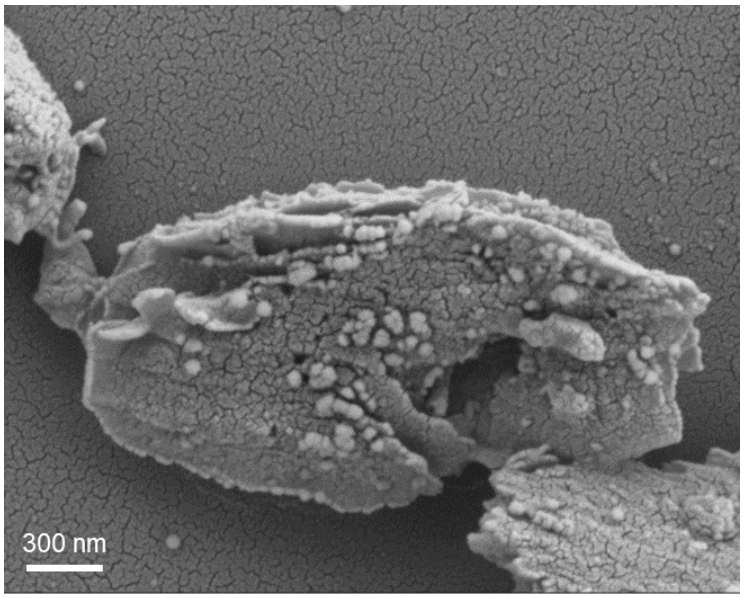

Fig. S6 SEM image of NCS-CoPt after stability test

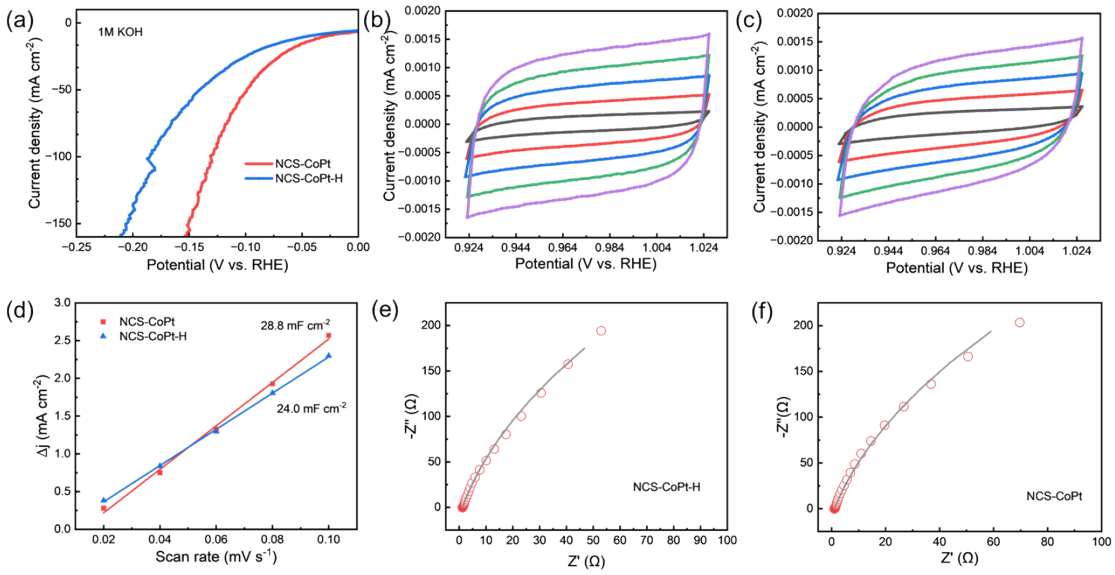

Fig. S7 (a) LSV cruves of NCS-CoPt, NCS-CoPt-H in 1 M KOH. (b-c) Cyclic voltammograms in 1 M KOH at the scan of 20-100 mV/s in non-faradaic region for NCS-CoPt, NCS-CoPt-H. (d) ECSA measurement of NCS-CoPt, NCS-CoPt-H. (e-f) Nyquist plot of NCS-CoPt, NCS-CoPt-H.

The HER activities of the catalysts were carried out in alkaline environment following the same test method to that in acidic media, except that the reference electrode was replaced with an Hg/HgO electrode. The overpotential required for NCS-CoPt and NCS-CoPt-H at a current density of 10 mA cm^{-2} were 31.4 mV and 47.8 mV in 1.0 M KOH (Fig S7a, ESI†), which were close to the results at 0.5 M H_2SO_4. However, the overpotentials required for the two catalysts were 98.9 mV, 130.0 mV (NCS-CoPt) and 141.0 mV, 185.3 mV (NCS-CoPt-H) at current densities of 50 mA cm^{-2} and 100 mA cm^{-2}, respectively, indicating a relatively lower catalytic activity in alkaline environments. The result of double-layer capacitance (C_{dl}) of two catalysts can be seen from Fig. S7 b-d (ESI†) that C_{dl} of NCS-CoPt (28.8 mF cm^{-2}) was larger to NCS-CoPt-H (24.8 mF cm^{-2}). Finally, the smaller R_{ct} value of NCS-CoPt (905 Ω) compared to that of NCS-CoPt-H (1370 Ω) demonstrated its better charge transfer capability (Fig. S7e-f, ESI†).

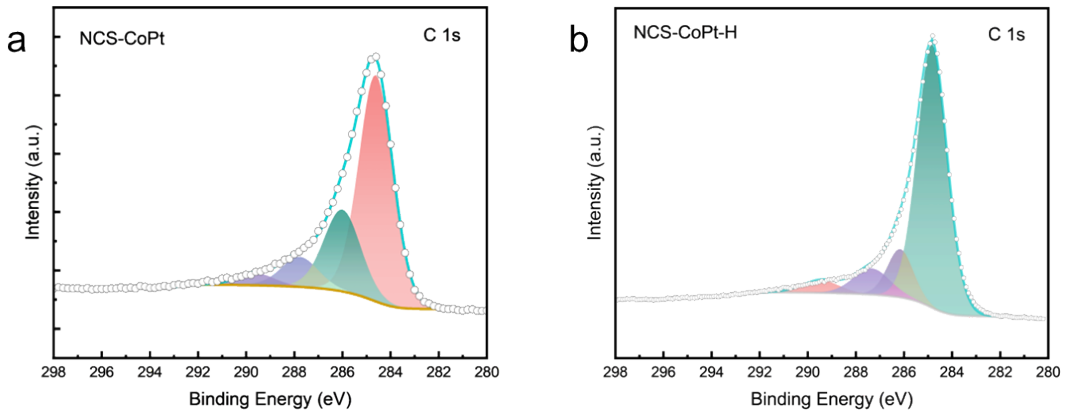

Fig. S8 High resolution of NCS-CoPt (a) and NCS-CoPt-H (b)

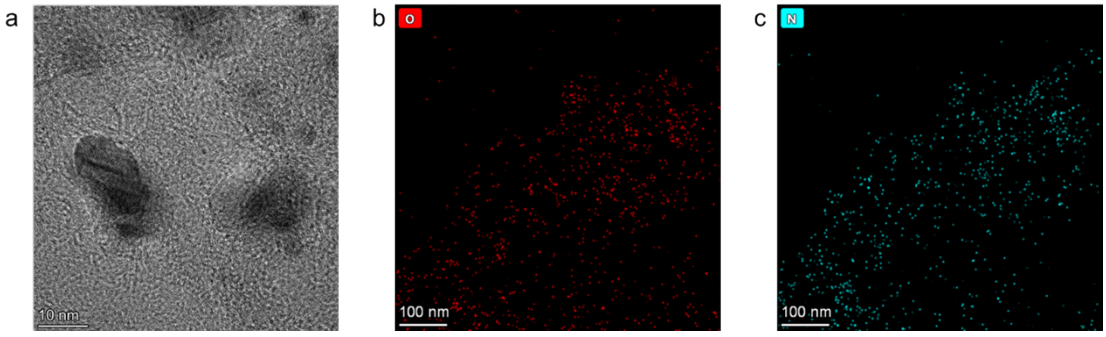

Fig. S9 TEM image and mapping of NCS-CoPt

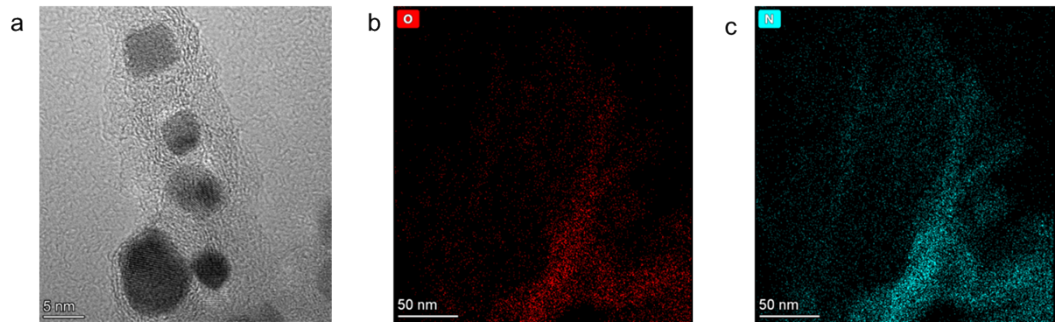

Fig. S10 TEM image and mapping of NCS-CoPt-H

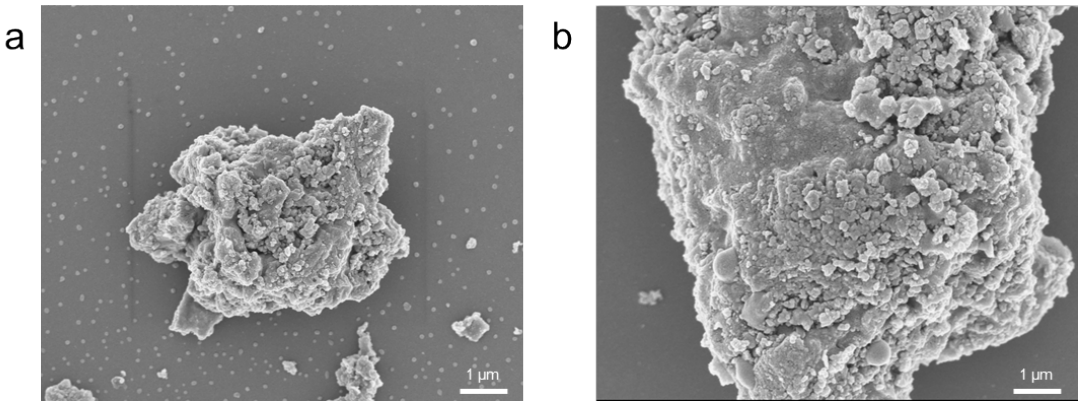

Fig. S11 SEM image of NCB-CoPt

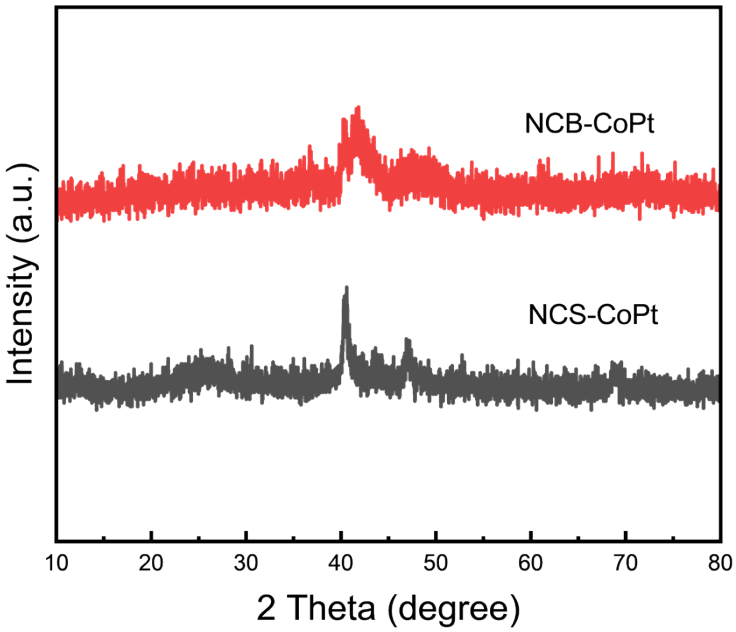

Fig. S12 XRD of NCS-CoPt and NCB-CoPt

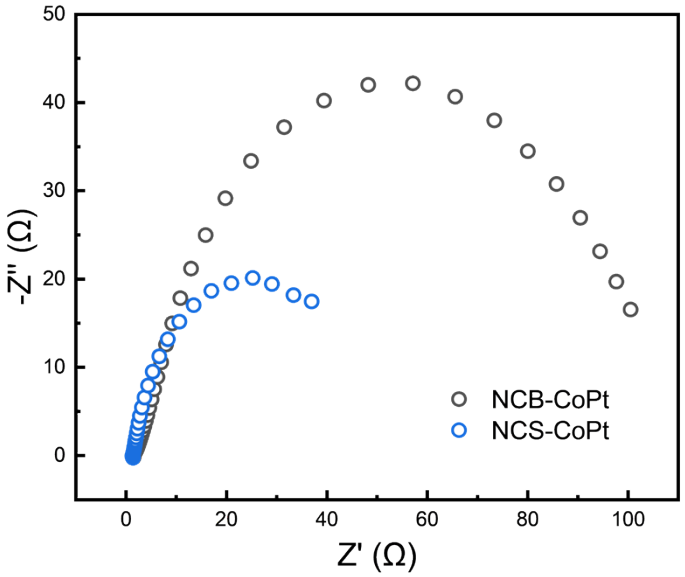

Fig. S13 Nyquist plot of NCB-CoPt and NCS-CoPt

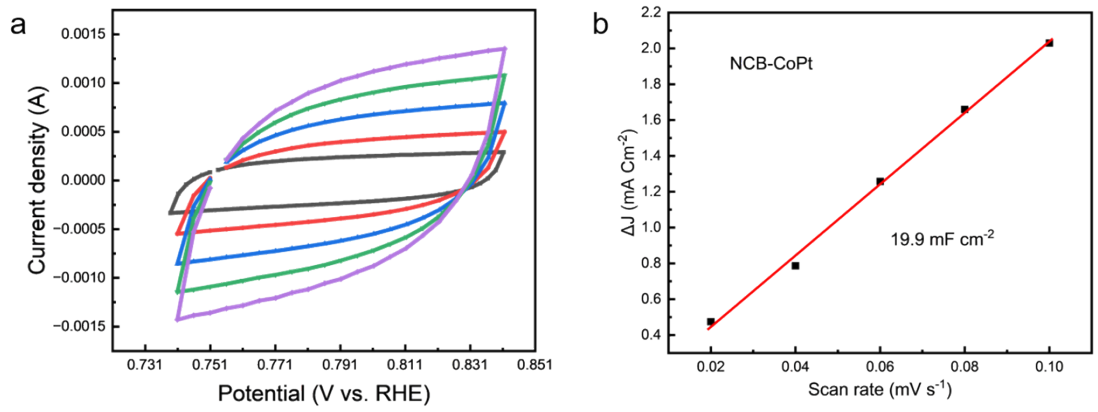

Fig. S14 (a) Cyclic voltammograms in 0.5 M H_2SO_4 at the scan of 20-100 mV s^{-1} in non-faradaic region for NCB-CoPt. (b) ECSA measurement of NCB-CoPt

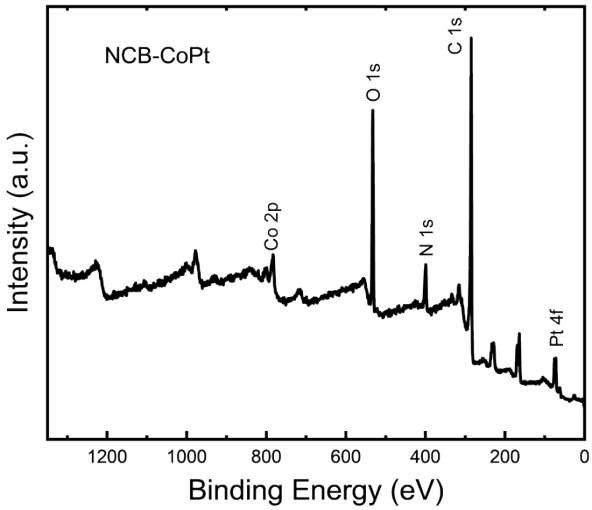

Fig. S15 XPS full survey spectrum of NCB-CoPt

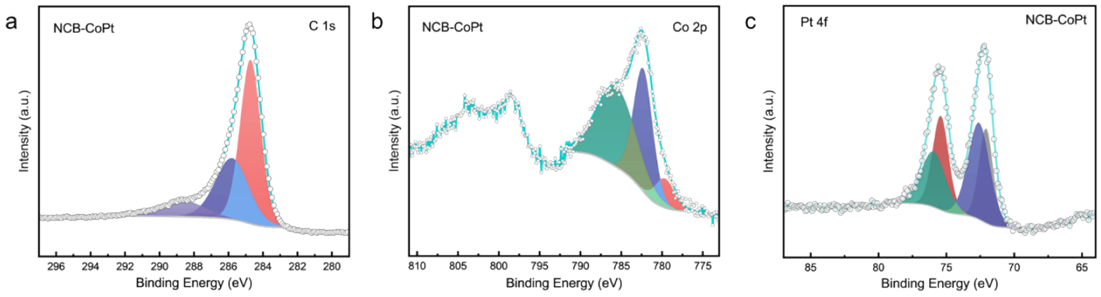

Fig. S16 High resolution of C 1s (a), Co 2p (b), and Pt 4f (c) spectra of NCB-CoPt

Table S1: Comparison of HER activities of different Carbon materials in 0.5 M H_2SO_4

Entry	Catalyst	Substrate	Overpotential for 10 mA cm^{-2} (mV)	Reference
1	NCS-CoPt	carbon paper	41	This work
2	NCS-CoPt-H	carbon paper	52	This work
3	Pt GDY2	glassy carbon	65	[3]
4	Pt@PCM	glassy carbon	105	[4]
5	5%Ru-MoS_2/CNT	glassy carbon	50	[5]
6	Ir@Co/NC	glassy carbon	60	[6]
7	Pt@FeNC	glassy carbon	60	[7]
8	PtN_x/TiO_2	glassy carbon	67	[8]
9	Pt SA/m-WO_{3-x}	glassy carbon	47	[9]
10	Pt-Ru dimer	glassy carbon	50	[10]
11	Pd NPs-Bis-24h	carbon paper	59.6	[11]
12	Pt-GT-1	glassy carbon	66	[12]

References

1. D. Gao, X. Wu, P. Wang, H. Yu, B. Zhu, J. Fan and J. Yu, Selenium-enriched amorphous $NiSe_{1+x}$ nanoclusters as a highly efficient cocatalyst for photocatalytic H_2 evolution, *Chem. Eng. J.*, 2021, **408**, 127230.
2. V. Wang, N. Xu, J.-C. Liu, G. Tang and W.-T. Geng, VASPKIT: A user-friendly interface facilitating high-throughput computing and analysis using VASP code, *Comput. Phys. Commun.*, 2021, **267**, 108033.
3. X.-P. Yin, H.-J. Wang, S.-F. Tang, X.-L. Lu, M. Shu, R. Si and T.-B. Lu, Engineering the Coordination Environment of Single-Atom Platinum Anchored on Graphdiyne for Optimizing Electrocatalytic Hydrogen Evolution, *Angew. Chem. Int. Ed.*, 2018, **57**, 9382-9386.
4. H. Zhang, P. An, W. Zhou, B. Y. Guan, P. Zhang, J. Dong and X. W. Lou, Dynamic traction of lattice-confined platinum atoms into mesoporous carbon matrix for hydrogen evolution reaction, *Sci. Adv.*, **4**, eaao6657.
5. X. Zhang, F. Zhou, S. Zhang, Y. Liang and R. Wang, Engineering MoS_2 Basal Planes for Hydrogen Evolution via Synergistic Ruthenium Doping and Nanocarbon Hybridization, *Adv. Sci.*, 2019, **6**, 1900090.
6. W.-H. Lai, L.-F. Zhang, W.-B. Hua, S. Indris, Z.-C. Yan, Z. Hu, B. Zhang, Y. Liu, L. Wang, M. Liu, R. Liu, Y.-X. Wang, J.-Z. Wang, Z. Hu, H.-K. Liu, S.-L. Chou and S.-X. Dou, General π-Electron-Assisted Strategy for Ir, Pt, Ru, Pd, Fe, Ni Single-Atom Electrocatalysts with Bifunctional Active Sites for Highly Efficient Water Splitting, *Angew. Chem. Int. Ed.*, 2019, **58**, 11868-

11873.

7. X. Zeng, J. Shui, X. Liu, Q. Liu, Y. Li, J. Shang, L. Zheng and R. Yu, Single-Atom to Single-Atom Grafting of Pt1 onto Fe-N_4 Center: Pt_1@Fe-N-C Multifunctional Electrocatalyst with Significantly Enhanced Properties, *Adv. Energy Mater.*, 2018, **8**, 1701345.

8. X. Cheng, Y. Lu, L. Zheng, Y. Cui, M. Niibe, T. Tokushima, H. Li, Y. Zhang, G. Chen, S. Sun and J. Zhang, Charge redistribution within platinum–nitrogen coordination structure to boost hydrogen evolution, *Nano Energy*, 2020, **73**, 104739.

9. J. Park, S. Lee, H.-E. Kim, A. Cho, S. Kim, Y. Ye, J. W. Han, H. Lee, J. H. Jang and J. Lee, Investigation of the Support Effect in Atomically Dispersed Pt on WO_{3-x} for Utilization of Pt in the Hydrogen Evolution Reaction, *Angew. Chem. Int. Ed.*, 2019, **58**, 16038-16042.

10. L. Zhang, R. Si, H. Liu, N. Chen, Q. Wang, K. Adair, Z. Wang, J. Chen, Z. Song, J. Li, M. N. Banis, R. Li, T.-K. Sham, M. Gu, L.-M. Liu, G. A. Botton and X. Sun, Atomic layer deposited Pt-Ru dual-metal dimers and identifying their active sites for hydrogen evolution reaction, *Nat. Commun.*, 2019, **10**, 4936.

11. H. Cheng, N. Yang, G. Liu, Y. Ge, J. Huang, Q. Yun, Y. Du, C.-J. Sun, B. Chen, J. Liu and H. Zhang, Ligand-Exchange-Induced Amorphization of Pd Nanomaterials for Highly Efficient Electrocatalytic Hydrogen Evolution Reaction, *Adv. Mater.*, 2020, **32**, 1902964.

12. J. N. Tiwari, S. Sultan, C. W. Myung, T. Yoon, N. Li, M. Ha, A. M. Harzandi, H. J. Park, D. Y. Kim, S. S. Chandrasekaran, W. G. Lee, V. Vij, H. Kang, T. J. Shin, H. S. Shin, G. Lee, Z. Lee and K. S. Kim, Multicomponent electrocatalyst with ultralow Pt loading and high hydrogen evolution activity, *Nat. Energy*, 2018, **3**, 773-782.